Comparative density-matrix renormalization group study of symmetry-protected topological phases in spin-1 chain and Bose-Hubbard models

Satoshi Ejima and Holger Fehske
Institut für Physik, Ernst-Moritz-Arndt-Universität Greifswald, 17487 Greifswald, Germany
(Received 22 July 2014; revised manuscript received 4 January 2015; published 16 January 2015)

We reexamine the one-dimensional spin-1 XXZ model with on-site uniaxial single-ion anisotropy as to the appearance and characterization of the symmetry-protected topological Haldane phase. By means of large-scale density-matrix renormalization group (DMRG) calculations the central charge can be determined numerically via the von Neumann entropy, from which the ground-state phase diagram of the model can be derived with high precision. The nontrivial gapped Haldane phase shows up in between the trivial gapped even Haldane and Néel phases, appearing at large single-ion and spin-exchange interaction anisotropies, respectively. We furthermore carve out a characteristic degeneracy of the lowest entanglement level in the topological Haldane phase, which is determined using a conventional finite-system DMRG technique with both periodic and open boundary conditions. Defining the spin and neutral gaps in analogy to the single-particle and neutral gaps in the intimately connected extended Bose-Hubbard model, we show that the excitation gaps in the spin model qualitatively behave just as for the bosonic system. We finally compute the dynamical spin structure factor in the three different gapped phases and find significant differences in the intensity maximum which might be used to distinguish these phases experimentally.

DOI: 10.1103/PhysRevB.91.045121 PACS number(s): 75.10.Pq, 64.70.Tg, 03.67.−a

I. INTRODUCTION

One-dimensional (1D) quantum spin systems have received continued attention as paradigms for strongly correlated systems, because miscellaneous—and even exotic—phases can be realized within simple model Hamiltonians. By way of example, the exactly solvable spin-1/2 antiferromagnetic (AFM) Heisenberg chain is known to be gapless, while for integer spins a gap exists between the ground state and the first excited state, as conjectured first by Haldane [1]. Especially for the spin-1 chain, the Haldane gap was confirmed experimentally [2,3], and the dynamical spin structure factor has been observed by inelastic neutron scattering, e.g., on $Ni(C_2H_8N_2)_2NO_2ClO_4$ [4]. Affleck, Lieb, Kennedy, and Tasaki (AKLT) proposed a exactly solvable model that offers valuable clues to the physics of the spin-1 Heisenberg chain [5]. The so-called AKLT state [cf. Fig. 1(a) below] successfully describes the ground state of the Haldane phase [6]. Also for the the spin-1 XXZ model, the ground-state phase diagram has been determined—even if a single-ion anisotropy is added [7]—e.g., by the Lanczos exact diagonalization (ED) technique based on the level spectroscopy method [8].

Currently, quantum integer-spin chains have attracted extraordinary interest from a topological point of view. The gapped ground states in the Haldane phase can be classified by the projective representations of the underlying symmetry group [9,10]. The odd Haldane (OH) phase in odd-integer-spin chains with two half-integer edge spins is a symmetry-protected topological (SPT) phase, because the odd-S AKLT state cannot be adiabatically connected to another trivial state without undergoing a phase transition. On the other hand, the even Haldane (EH) state in the even-integer-spin systems with integer edge spins [11–14] is a trivial state, since the even-S AKLT state is adiabatically connected to a trivial state without a bulk phase transition [15,16].

Interestingly, a hidden SPT phase analogous to the OH phase was discovered in the extended Bose-Hubbard model (EBHM) with longer-range repulsions [17]. This Haldane-insulator (HI) phase, embedded between the Mott-insulator (MI) and the density-wave (DW) phases in the intermediate coupling regime, exhibits the characteristic degeneracy of the entanglement spectrum in the Haldane phase [18]. The excitation gaps at the quantum phase transition lines depend on their universality classes [17,19]. Beyond that, the dynamical density structure factor $S_{\mathrm{EBHM}}(k,\omega)$ significantly differs in the MI, DW, and HI states [18].

On the basis of our recent EBHM study [18], in the present work we investigate the topological properties of the odd Haldane phase in the anisotropic spin-1 XXZ chain which, as we will show, can be taken as an effective model for the EBHM. Using the density-matrix renormalization group (DMRG) technique [20–22], first we determine the phase boundaries by exploiting the central charge. In order to confirm the closing of the excitation gap at the trivial-nontrivial phase transition points, we simulate both the spin and neutral gaps. We furthermore demonstrate the degeneracy of entanglement levels in the OH phase with both periodic (P) and open (O) boudary conditions (BC) (for the anisotropic spin-1 XXZ chain it is well known how the edge spins should be treated in the latter case). In order to experimentally detect the topological HI phase in the EBHM, various dynamical quantities have been proposed [17,18,23]. Here we will examine the dynamical spin structure factor $S^{zz}(k,\omega)$ for the spin-1 model by means of the dynamical DMRG (DDMRG) technique [24]. We will demonstrate that the intensity maximum in $S^{zz}(k,\omega)$ features a gapped dispersion in the nontrivial Haldane phase as obtained for $S_{\mathrm{EBHM}}(k,\omega)$ in the EBHM. Since this quantity is directly accessible by inelastic neutron scattering, significant differences in $S^{zz}(k,\omega)$ could be used to detect the various gapped phases.

This paper is organized as follows. In the next section we establish the anisotropic spin-1 XXZ model and the corresponding EBHM. The physical quantities of interests are

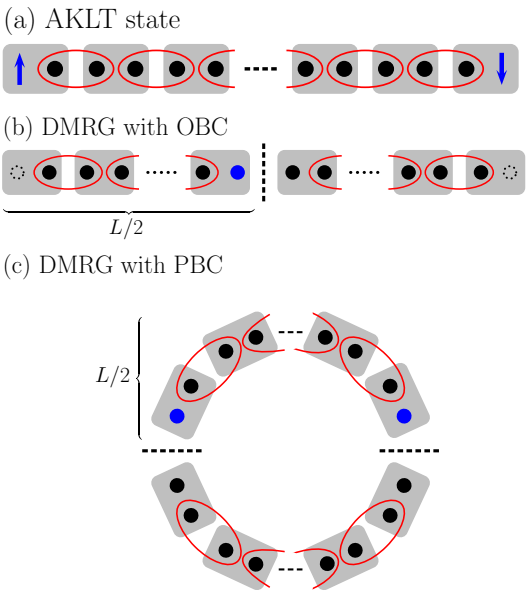

FIG. 1. (Color online) (a) Valence bond picture of the AKLT state in a spin-1 XXZ chain. Each of the two $S = 1/2$ spins connected by an ellipse form a singlet $(1/\sqrt{2})(\uparrow\downarrow - \downarrow\uparrow)$. The two free edge spins cause the fourfold degeneracy of the ground-state energy. (b) To simulate the AKLT state within OBC DMRG, the free edge spins have to be excluded from the system (dashed circles). (c) With PBC the AKLT state can be simulated without any changes, so that the lowest entanglement level exhibits a fourfold degeneracy according to the two edge spins.

introduced in Sec. III. Large-scale (D) DMRG results for the anisotropic spin-1 XXZ chain will be presented and discussed in Sec. IV. Section V contains a brief summary and our main conclusions.

II. MODEL HAMILTONIANS

In this section we introduce the anisotropic spin-1 XXZ model and get back to its established ground-state phase properties. We then define the extended Bose-Hubbard model and point out the correspondences with an effective spin-1 XXZ model.

A. Spin-1 XXZ model with single-ion anisotropy

The Hamiltonian of the 1D spin-1 XXZ model with on-site anisotropy is given by

$$\hat{\mathcal{H}} = \sum_j \left[J\left(\hat{S}_j^x \hat{S}_{j+1}^x + \hat{S}_j^y \hat{S}_{j+1}^y\right) + J_z \hat{S}_j^z \hat{S}_{j+1}^z \right] + D \sum_j \left(\hat{S}_j^z\right)^2, \tag{1}$$

where $\hat{\boldsymbol{S}}_j$ denotes a spin-1 operator. The parameter D represents the uniaxial single-ion anisotropy. The ground-state phase diagram of the model (1) exhibits various gapful and gapless phases, namely, following the conventional notations, the Haldane phase, the large-D phase, two XY phases, the ferromagnetic phase, and the Néel phase [7,25,26]. According to this, different types of phase transitions occur between these phases: (i) A gapful-gapful Gaussian phase transition takes place between the large-D phase and the Haldane phase with the central charge $c = 1$, (ii) the Haldane-Néel transition appears to be of the Ising universality class with $c = 1/2$, and (iii) a gapless-gapful Berezinskii-Kosterlitz-Thouless (BKT) transition emerges between the XY phase and the Haldane or large-D phase. In what follows we restrict ourselves to the parameter region where $J_z > 0$ and $D > 0$. Following the notation by Kjäll *et al.* [16], we use the termini EH, OH, and AFM phases instead of the large-D, Haldane, and Néel phases, respectively. The lattice-inversion symmetry, which protects the SPT state of the Haldane phase, can be broken by adding a perturbation to the Hamiltonian (1):

$$\delta\hat{\mathcal{H}} = g \sum_j \left[\hat{S}_j^z \left(\hat{S}_j^x \hat{S}_{j+1}^x + \hat{S}_j^y \hat{S}_{j+1}^y\right) - \hat{S}_{j+1}^z \left(\hat{S}_j^x \hat{S}_{j+1}^x + \hat{S}_j^y \hat{S}_{j+1}^y\right) + \text{H.c.} \right]. \tag{2}$$

Any finite g immediately lifts the characteristic degeneracy of the lowest entanglement level in the Haldane phase [10]. As we will see later, thereby the EH-OH quantum phase transition also disappears.

B. Extended Bose-Hubbard model

In 2006, Dalla Torre *et al.* [17] discovered the HI phase in the 1D extended Bose-Hubbard model with longer-range repulsions. The HI phase features the properties of the OH phase in the spin-1 model (1). The EBHM Hamiltonian reads

$$\hat{\mathcal{H}}_{\text{EBHM}} = -t \sum_j (\hat{b}_j^\dagger \hat{b}_{j+1} + \text{H.c.}) + U \sum_j \hat{n}_j(\hat{n}_j - 1)/2 + V \sum_j \hat{n}_j \hat{n}_{j+1}, \tag{3}$$

where $\hat{b}_j^\dagger$ ($\hat{b}_j$) creates (annihilates) a boson at lattice site j, and $\hat{n}_j = \hat{b}_j^\dagger \hat{b}_j$ is the corresponding boson number operator. The nearest-neighbor boson transfer amplitude is given by t and U (V) parametrizes the on-site (nearest-neighbor) particle repulsion. Assuming that the site occupation is restricted to $n_j = 0$, 1, or 2, with $S_j^z = n_j - 1$ for a mean boson filling factor $\rho = N/L = 1$, the system can be mapped onto an effective spin-1 Hamiltonian,

$$\hat{\mathcal{H}}_{\text{EBHM}}^{\text{eff}} = \hat{\mathcal{H}} + \hat{\mathcal{H}}', \tag{4}$$

with the replacements $J \to -t$, $J_z \to V$, and $D \to U/2$ in Eq. (1). $\hat{\mathcal{H}}'$ contains further terms which breaks the particle-hole symmetry of $\hat{\mathcal{H}}$ [see Eq. (A1) of Ref. [19] for the explicit form of $\hat{\mathcal{H}}'$]. The EBHM exhibits three insulating phases, where the nontrivial HI phase appears in between the MI and DW phases for intermediate couplings. The MI, HI, and DW phases of the EBHM correspond to the EH, OH, and AFM phases of the spin-1 model (1), respectively.

III. PHYSICAL QUANTITIES OF INTEREST

In this section we assort the quantities that can be used to characterize the different phases and phase transitions in the spin-1 model (1) and accordingly in the EBHM. We furthermore explain how the quantities can be simulated using the DMRG technique.

A. Entanglement spectrum, von Neumann entropy, and central charge

After Li and Haldane's proposal [27] to characterize topological phases by the entanglement spectrum, this has become one of the most powerful tools to investigate the SPT state. Dividing a system with L sites into two subblocks and considering the reduced density matrix $\rho_\ell = \mathrm{Tr}_{L-\ell}[\rho]$ of a subblock of arbitrarily length ℓ, the entanglement spectrum ξ_α is obtained from the weights λ_α of the reduced density matrix ρ_ℓ by

$$\xi_\alpha = -2\ln\lambda_\alpha. \tag{5}$$

The entanglement spectrum of a subblock with $\ell = L/2$ sites can be obtained for OBC and PBC as sketched in Figs. 1(b) and 1(c), respectively. Thereby the artificial edges give rise to the characteristic degeneracy of the lowest entanglement level in the nontrivial AKLT state [displayed in Fig. 1(a)], where the degree of degeneracy depends on the boundary conditions. To determine the entanglement spectrum in the OH phase with OBC, a well-known trick is in use: One simulates a system without free edge spins by replacing the edge sites with $S = 1/2$, as shown in Fig. 1(b). One then expects a doubly degenerate lowest entanglement level in the OH phase. For PBC, on the other hand, for the same finite system, a fourfold degeneracy is expected due to two free $S = 1/2$ spins [see Fig. 1(c)], just as for the HI phase in the EBHM [18].

The entanglement analysis provides also valuable information about the criticality of the system. Adding up the λ_α during the simulation, we have direct access to the von Neumann entropy $S_L(\ell) = -\mathrm{Tr}_\ell[\rho_\ell \ln \rho_\ell]$. From conformal field theory [28], it follows that in the case of a periodic system the von Neumann entropy takes the form

$$S_L(\ell) = \frac{c}{3}\ln\left[\frac{L}{\pi}\sin\left(\frac{\pi\ell}{L}\right)\right] + s_1, \tag{6}$$

where s_1 is a nonuniversal constant. Since the most precise data of $S_L(\ell)$ are obtained when the length ℓ of the subblock equals half the system size L, the relation [29]

$$c^*(L) \equiv \frac{3[S_L(L/2-1) - S_L(L/2)]}{\ln[\cos(\pi/L)]} \tag{7}$$

is much better suited for determining the central charge than directly using the above expression for $S_L(\ell)$.

For the EBHM the phase boundaries can be assigned very effectively using the (numerically determined) central charge c^*, because the system becomes critical only at the MI-HI (HI-DW) transition points where $c = 1$ ($c = 1/2$), and there c^* shows pronounced peaks [18]. Hence we adopt this method for the spin-1 model (1) as well to pinpoint the EH-OH and OH-AFM transition points.

B. Excitation gaps

Monitoring various excitation gaps for the EBHM, significant features have been found at the MI-HI and HI-DW transition points [17,19]. For example, the single-particle gap,

$$\Delta_c = E_0^{\mathrm{EBHM}}(N+1) + E_0^{\mathrm{EBHM}}(N-1) - 2E_0^{\mathrm{EBHM}}(N), \tag{8}$$

is finite in all three insulating phases, except for the MI-HI transition point. By contrast, the neutral gap,

$$\Delta_n = E_1^{\mathrm{EBHM}}(N) - E_0^{\mathrm{EBHM}}(N), \tag{9}$$

closes at both the MI-HI and HI-DW transitions. In Eqs. (8) and (9), $E_0^{\mathrm{EBHM}}(N)$ and $E_1^{\mathrm{EBHM}}(N)$ denote the energies of the ground state and first excited state of the N-particle system for the EBHM, respectively.

Since adding (removing) a particle in the EBHM corresponds to raising (lowering) the spin S^z projection in a pseudospin model, we consider for the spin-1 XXZ model the spin gap

$$\Delta_s = E_0^{XXZ}(1) - E_0^{XXZ}(0), \tag{10}$$

which likewise might be finite in all three phases, except for the EH-OH transition point. As for the EBHM, the neutral gap in the spin-1 model (1) can be defined as

$$\Delta_n = E_1^{XXZ}(0) - E_0^{XXZ}(0), \tag{11}$$

where $E_0^{XXZ}(M)$ and $E_1^{XXZ}(M)$ denote the ground-state and first excited energies within the subspace $M = \sum_j S_j^z$, respectively. By analogy to the behavior of the neutral gap in the EBHM, Δ_n should vanish at the EH-OH and OH-AFM transition points for the spin-1 chain model.

C. Dynamical spin structure factor

Simulating the dynamical spin structure factor by DDMRG is of particular importance since it might be directly compared with inelastic neutron scattering experiments, e.g., on $Ni(C_2H_8N_2)_2NO_2ClO_4$ [4]. Its zz component is defined by

$$S^{zz}(k,\omega) = \sum_n \left|\langle\psi_n|\hat{S}_k^z|\psi_0\rangle\right|^2 \delta(\omega-\omega_n), \tag{12}$$

where $|\psi_0\rangle$ and $|\psi_n\rangle$ denote the ground state and nth excited state, respectively. The corresponding excitation energy is $\omega_n = E_n - E_0$. For $D = 0$, i.e., for the isotropic Heisenberg or XXZ fix points of (1), $S^{zz}(k,\omega)$ was extensively studied by ED [30] and time-dependent DMRG [31] techniques. That is, the behavior of $S^{zz}(k,\omega)$ in the Haldane phase is well known, albeit numerical results for the EH and AFM states are rare. Taking into account the relation $S_j^z = n_j - \rho$ for the pseudospin in the effective model $\hat{\mathcal{H}}_{\mathrm{EBHM}}^{\mathrm{eff}}$, one expects that the spin structure factor $S^{zz}(k,\omega)$ corresponds to the dynamical density structure factor $S_{\mathrm{EBHM}}(k,\omega)$ in the EBHM, which exhibits different behavior in the three insulating phases [18].

IV. NUMERICAL RESULTS

In this section we present our numerical (D)DMRG results for the spin-1 XXZ model with and without single-ion anisotropy. We first determine the phase boundaries and then analyze the behavior of the excitation gaps at the transitions between the nontrivial and trivial phases. Furthermore, we discuss the entanglement spectra of an odd Haldane phase. Finally, we simulate the dynamic spin structure factor and compare it with the dynamical density response in the EBHM.

In the numerics we keep up to $m = 3200$ density-matrix states for the static DMRG runs, so that the discarded weight is

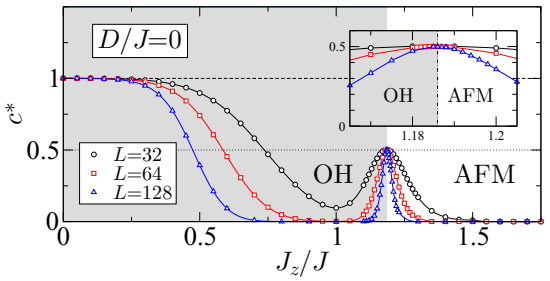

FIG. 2. (Color online) Central charge $c^*(L)$ as obtained by DMRG for the spin-1 XXZ model with $D = 0$ and PBC. The OH-AFM transition can be assigned to $J_z/J = 1.186 \pm 0.001$ with $c = 1/2$, where a pronounced peak appears [see also the magnifying inset which shows $c^*(L)$ close to the transition point].

typically smaller than 1×10^{-10}. For the DDMRG simulations we take $m = 800$, examining the ground state along the first five DMRG sweeps, and then use $m = 400$ states computing dynamical properties.

A. Phase boundaries

1. OH-AFM transition

Let us first discuss the spin-1 model (1) with $D = 0$. In this case it is known that a BKT transition occurs at $J_z = 0$ between the XY and OH phases [32]. At $J_z > 0$, only an OH-AFM transition takes place, where $c = 1/2$ is expected.

Figure 2 shows the central charge $c^*(L)$, computed from Eq. (7). If J_z/J is raised at fixed system size, the maximum in $c^*(L)$ sharpens at the OH-AFM transition point $J_{z,c1}/J$, and we deduce $c^* \simeq 0.5$. The other critical point $J_{z,c2}/J \simeq 1.185$ with $c^* \simeq 0.503$ approximates the recent infinite-system DMRG result $J_{z,c2}/J = 1.186 \pm 0.002$ [16,33] very well already for $L = 32$. The agreement becomes perfect if we increase the system size: $J_{z,c2}/J \simeq 1.186$ with $c^* \simeq 0.500$ for $L = 128$. Note that $c^*(L)$ stays equal to one in a relatively wide region (from $J_z/J = 0$ to $J_z/J \simeq 0.3$ for $L = 128$), indicating the BKT transition between the XY and the OH phases at $J_z/J = 0$ with $c = 1$.

To relate our numerical results to previous ones we include an on-site anisotropy D and compute $c^*(L)$ in the vicinity of the OH-AFM transition. For $D/J = 0.5$ the central charge $c^*(L)$ at fixed system size L develops again a pronounced maximum at the OH-AFM transition point [see Fig. 3(a)]. The deduced transition point $J_{z,c1}/J(L)$ is readily extrapolated to the thermodynamic limit [Fig. 3(b)], yielding $J_{z,c2}/J \simeq 1.4897$, which is in reasonable agreement with the ED result $J_{z,c2}/J \simeq 1.536$ obtained from systems with L up to 16 [7] and confirms recent DMRG data $J_{z,c2}/J = 1.4905 \pm 0.0015$ [34].

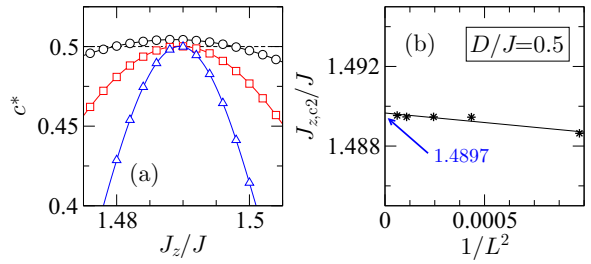

FIG. 3. (Color online) $c^*(L)$ for $D = 0.5$ near the OH-AFM transition. (b) shows that the Ising transition point $J_{z,c2}/J(L)$ obtained from $c^*(L)$ can be linearly extrapolated to the thermodynamic limit.

2. EH-OH transition

We now turn to the case $D > 0$. In previous works [7,32,35,36] a Gaussian transition between the EH and OH phases has been found by employing the level spectroscopy technique to ED results obtained for small systems. Applying the twisted boundary conditions (TBC), $\hat{S}^x_{L+1} = -\hat{S}^x_1$, $\hat{S}^y_{L+1} = -\hat{S}^y_1$, and $\hat{S}^z_{L+1} = \hat{S}^z_1$ within DMRG, the two lowest energy levels can be simulated accurately for much larger system sizes than accessible to ED. Figure 4(a) demonstrates that the two lowest energies assigned to the EH and OH states cross at $J_{z,c1}/J \simeq 1.6945$ by increasing J_z/J at fixed $D/J = 1.5$ for $L = 32$ (and TBC). The critical points $J_{z,c1}/J(L)$ can be systematically extrapolated to the thermodynamic limit by a linear fit, as indicated in Fig. 4(b). For $L \to \infty$ we obtain $J_{z,c1}/J \simeq 1.6938$.

Alternatively, the EH-OH transition points can be extracted from the central charge $c^*(L)$ if compared with the field theoretical prediction $c = 1$. This is demonstrated in Fig. 4(c).

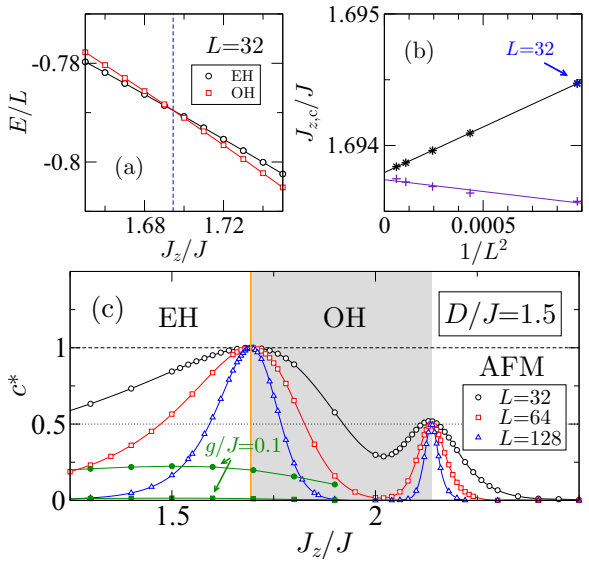

FIG. 4. (Color online) (a) J_z dependence of the two lowest energy eigenvalues at $D/J = 1.5$, using TBC and $L = 32$. Obviously the energies of the OH state (squares) and the EH state (circles) cross at the EH-OH transition point (dashed line). (b) Critical points $J_{z,c1}/J$ obtained by the level spectroscopy technique (stars) [via the central charge (pluses)] as obtained in (a) [(c)] vs the inverse of the system size squared at $D/J = 1.5$ for L up to 128. (c) Central charge c^* of the 1D spin-1 XXZ model (1) with $D/J = 1.5$, indicating the EH-OH (OH-AFM) transition point with $c = 1$ ($c = 1/2$). The solid line denotes the EH-OH transition extracted from (a) and (b), which is in accordance with the position of the maximum in $c^*(L)$. Turning on a perturbation $\delta\hat{\mathcal{H}}$ that breaks the lattice-inversion symmetry, the central charge $c^*(L)$ (solid symbols) becomes zero for large enough system sizes ($L \geqslant 64$).

Here the maxima of $c^*(L)$ can also be extrapolated to the thermodynamic limit [see Fig. 4(b)], where the transition point is in excellent accord with the ones via level spectroscopy in Figs. 4(a) and 4(b). We note that also the OH-AFM transition can be reliably determined from the peak at $J_{z,c2}/J \simeq 2.138$.

B. Characterization of the topological phase

In the following we analyze the signatures of the topological OH phase and of the transition between the trivial and nontrivial topological states for the model (1) in close analogy to the EBHM [18]. To this end, we simulate the excitation gaps and the entanglement spectra.

1. Excitation gaps

So far the excitation gaps of (1) have been studied mostly at the isotropic Heisenberg point with respect to the magnitude of the Haldane gap. At the trivial-nontrivial phase transition points the excitation gaps should close, as demonstrated, e.g., for the EBHM [17,19]. Here we compute the spin and neutral excitation gaps as defined in Sec. III B instead of calculating the simple first excitation gap. Thereby, we adopt PBC instead of OBC within DMRG, avoiding the use of edge spins, which have to be adapted according to the considered parameter region.

Figure 5(a) shows first the excitation gaps at $D = 0$. Upon increasing J_z/J, the gaps open exponentially, reflecting the BKT transition at $J_z/J = 0$. Δ_n and Δ_s cross each other exactly at the Heisenberg point, $J_z/J = 1$, where $\Delta_n(L) = \Delta_s(L)$ (see the discussion about the system-size dependence of the excitation gaps and the magnitude of the Haldane gap for the spin-1 Heisenberg model in the Appendix). At the OH-AFM transition ($J_{z,c}/J \simeq 1.186$), Δ_n closes linearly

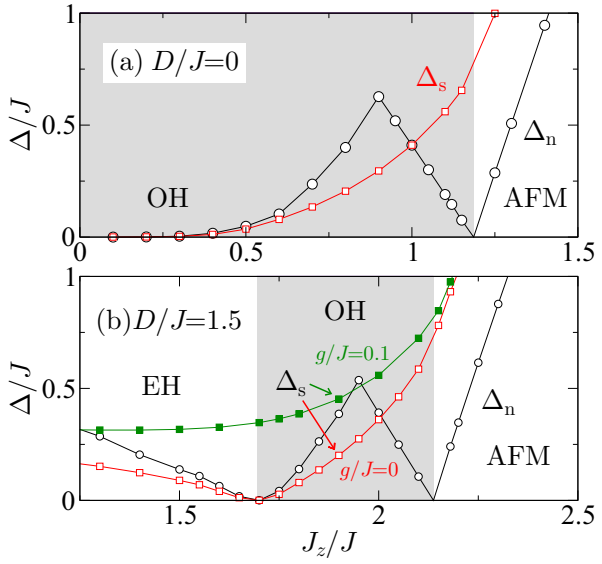

FIG. 5. (Color online) Extrapolated data for the spin gap Δ_s (squares) and neutral gap Δ_n (open circles) as a function of J_z/J for (a) $D/J = 0$ and (b) $D/J = 1.5$. The solid squares in (b) give Δ_s with a finite inversion-symmetry-breaking perturbation $g/J = 0.1$ [see Eq. (2)].

because the transition belongs to the Ising universality class, while Δ_s remains finite.

For $D/J = 1.5$ [see Fig. 5(b)], the EH-OH transition occurs at $J_{z,c1}/J \sim 1.6938$, where both spin and neutral gaps vanish. Increasing J_z/J above $J_{z,c1}/J$, only Δ_n closes at the Ising transition point $J_{z,c2}/J$, just as in the case of $D/J = 0$ [compare Figs. 5(a) and 5(b)]. If we turn on the perturbation $\delta\hat{\mathcal{H}}$ [see Eq. (2)], which breaks the lattice-inversion symmetry explicitly, the EH-OH transition disappears, so that Δ_s stays finite for $g/J = 0.1$, as shown in Fig. 5(b). Thereby, owing to the loss of the criticality at the EH-OH transition, $c^*(L)$ converges to zero for large enough L, as demonstrated in Fig. 4(c).

Comparing the behavior of the excitation gaps with those of the EBHM [17,19], one sees that the spin (neutral) gap in the spin-1 model (1) takes the role of the single-particle (neutral) gap in the EBHM.

2. Entanglement spectra

Let us now analyze the entanglement properties of the topological states for intermediate single-ion anisotropy ($D/J = 1.5$), where both the EH-OH and OH-AFM transitions exist. Here Pollmann *et al.* [10] showed that the SPT state in the OH phase has a twofold degenerate lowest entanglement level for the quantum spin chain model. The infinite-time evolving block decimation procedure used by those authors gives the entanglement spectra data directly in the thermodynamic limit. In the following we show that when simulating the model (1) for a finite system by conventional DMRG, this characteristic degeneracy of the OH phase can also be obtained, but the degree of the degeneracy depends on the boundary conditions.

Figure 6 presents the entanglement spectrum ξ_α for the anisotropic spin-1 XXZ model with $D/J = 1.5$. For a small system ($L = 64$) with PBC [Fig. 6(a)] the lowest entanglement level is fourfold degenerate only deep inside the OH phase. This reflects the possession of the two edges for the subblock $L/2$. Increasing the system size, this degeneracy is observed for a larger region of the OH phase, as demonstrated by Fig. 6(b) for $L = 128$, but close to the EH-OH transition point the lowest entanglement level is still nondegenerate. To overcome this drawback we apply OBC with half-spin edges in the OH phase [cf. Fig. 1(b)]. The same procedure has been used to estimate the magnitude of the Haldane gap at the isotropic Heisenberg point. Figure 6(c) gives ξ_α for $L = 128$ and OBC, pointing out the twofold degeneracy of the lowest level in the nontrivial phase and its nondegeneracy anywhere else. The degeneracy is clearly caused by the single edge spin of subblock $L/2$.

Recently it has been demonstrated for quantum spin chains [10] and the EBHM [18] that the degeneracy of the lowest entanglement level in the OH phase might be lifted by turning on an inversion-symmetry-breaking term, such as (2). Figure 7(a) [Figure 7(c)] exemplifies that the fourfold [twofold] degeneracy with PBC [OBC] indeed dissolves for any finite g. Thereby, the gap between the lowest levels becomes larger as g increases—see Fig. 7(b) [Fig. 7(d)] for PBC [OBC]. Obviously inversion symmetry protects the Haldane phase.

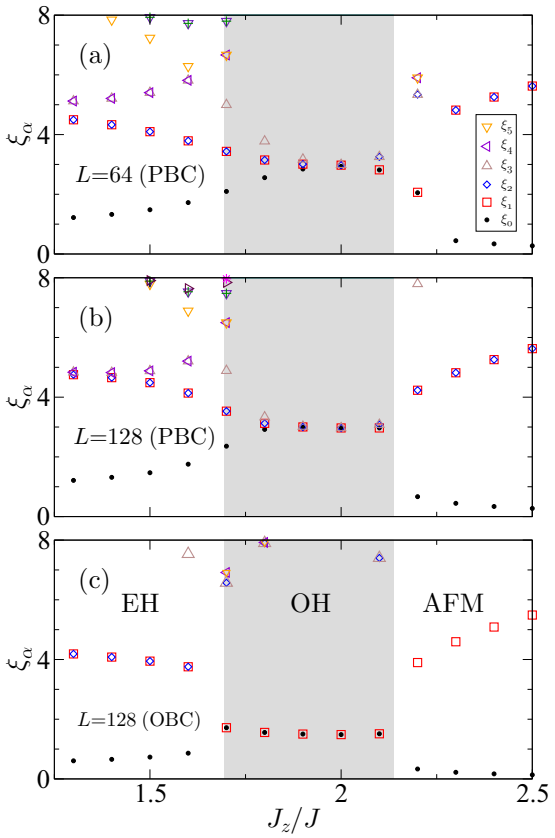

FIG. 6. (Color online) Entanglement spectrum ξ_α of the 1D spin-1 XXZ model (1) with $D = 1.5$. The fourfold degeneracy of the lowest entanglement level can be taken as an indication of a nontrivial Haldane state in the case of DMRG simulations with PBC. As the system size increases, the degeneracy appears in the whole HI phase; compare data for $L = 64$ [(a)] with those for 128 [(b)]. Using OBC and taking spins ($S = 1/2$) at the edges into account, an almost perfect double degeneracy is obtained for the OH phase even for small systems with $L = 128$, as demonstrated in (c).

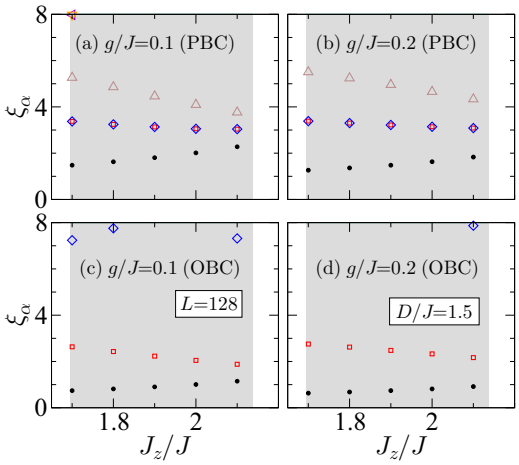

FIG. 7. (Color online) Entanglement spectrum ξ_α if an inversion-symmetry-breaking term is added to the spin-1 chain (1) with $D = 1.5$, where $g/J = 0.1$ (left panels) and 0.2 (right panels). Data obtained by DMRG with PBC (upper panels) and OBC with half-spin edges (lower panels).

3. *Multicritical point and EH-AFM transition*

Raising the ratios D/J and J_z/J, the EH-OH and OH-AFM critical lines merge at the multicritical point $(J_{z,\mathrm{mc}}/J, D_{\mathrm{mc}}/J)$. Above this point, i.e., for $J_z > J_{z,\mathrm{mc}}$ and $D > D_{\mathrm{mc}}$, a direct EH-AFM transition is expected to occur, as pointed out by den Nijs and Rommeles [26]. This has been confirmed numerically by ED, yielding $(J_{z,\mathrm{mc}}, D_{\mathrm{mc}}) \approx (3.2, 2.9)$ [7]. It is challenging to determine this multicritical point more precisely, but the entanglement analysis outlined above seems to be a powerful tool. Obviously, for fixed values $D > D_{z,\mathrm{mc}}$, the lowest entanglement level is nondegenerate for the whole parameter regime of J_z/J including the EH-AFM transition point, while for $D < D_{\mathrm{mc}}$ the lowest entanglement level should be degenerate for a very narrow but finite parameter region of J_z/J. In fact, the double degeneracy can still be observed at $D/J = 2.88$ by large-scale DMRG simulations with $L = 1024$ and OBC [see Fig. 8(a)]. If D/J is increased slightly, the degeneracy is lifted for $L = 1024$ [see Fig. 8(b) for $D/J = 2.9$], but from the results presented we cannot derive a definite conclusion about what happens for $L \to \infty$. Figure 8(c) indicates that degeneracy disappears already at $D/J = 2.92$. In this way the ED results regarding the existence of the multicritical point is corroborated by our more precise entanglement spectra analysis, yielding $(J_{z,\mathrm{mc}}/J, D_{\mathrm{mc}}/J) = (3.196 \pm 0.02, 2.90 \pm 0.02)$.

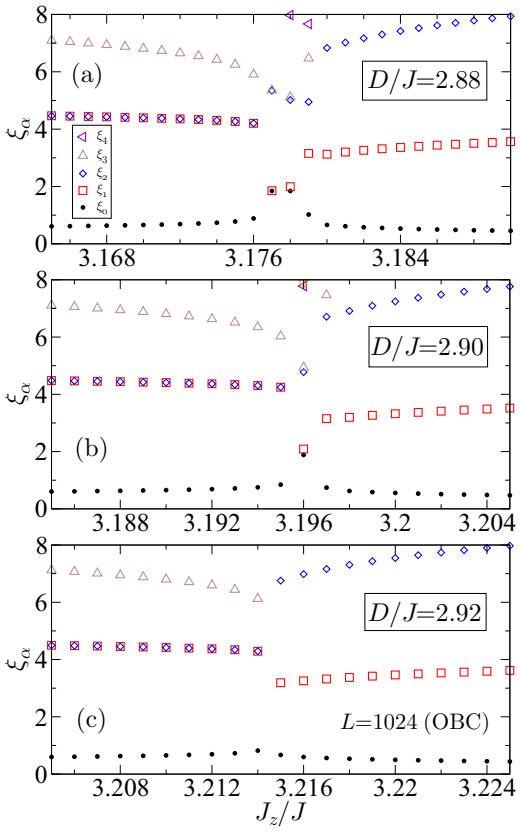

FIG. 8. (Color online) Entanglement spectrum ξ_α for (a) $D/J = 2.88$, (b) 2.90, and (c) 2.92 close to the EH-OH-AFM multicritical point with $L = 1024$ and OBC, showing the disappearance of the double degeneracy of the lowest entanglement levels.

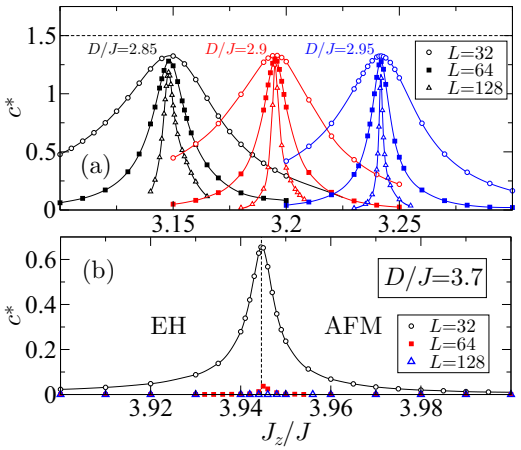

FIG. 9. (Color online) Central charge c^* of the 1D spin-1 XXZ model (1), (a) near the multicritical point $D_{\rm mc}/J$ and (b) across the first-order EH-AFM transition for $D/J = 3.7$. The dashed line in (b) denotes the EH-AFM transition point $D/J \simeq 3.9446$ according to Ref. [33].

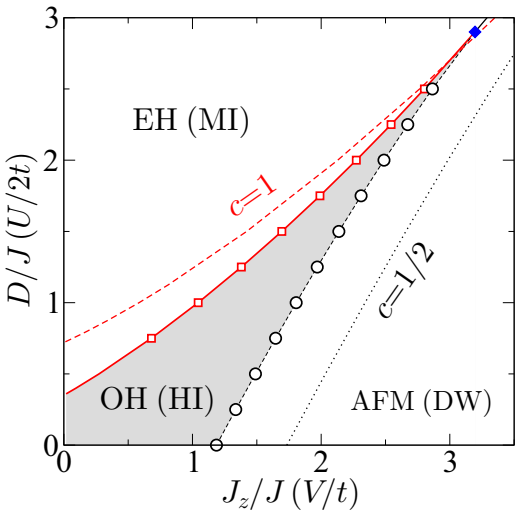

FIG. 10. (Color online) DMRG ground-state phase diagram of the 1D spin-1 XXZ model with single-ion anisotropy (1). Shown are the even Haldane (EH), odd Haldane (OH), and antiferromagnetic (AFM) phases. The EH-OH (squares) and OH-AFM (circles) transition points are determined from the central charge $c = 1$ and $c = 1/2$, respectively, which was extracted from the von Neumann entropy via Eq. (7). The EH-OH transition line was confirmed by a careful finite-size scaling of the two low-lying energy levels with TBC. The solid diamond gives the EH-OH-AFM multicritical point determined from the entanglement analysis. Error bars are smaller than symbols. The dashed (dotted) line denotes the MI-HI (HI-DW) transition in the EBHM with $n_b = 2$ bosons per site (taken from Ref. [18]).

Certainly it is of great interest to look at the behavior of the central charge at the multicritical point. Here the central charge might be $c = 1 + 1/2 = 3/2$ because BKT- and Ising-transition lines merge. Figure 9(a) displays the numerically obtained central charge $c^*(L)$ for fixed values of D/J in the vicinity of the multicritical point. We see that $c^*(L)$ is always smaller than 3/2 and decreases with increasing system size L. Unfortunately, the system-size dependence of $c^*(L)$ is much stronger than those, e.g., at $D/J = 1.5$, in Fig. 4; so it turns out that even $L = 128$ is not large enough to precisely determine the value of the central charge. Maybe the use of the infinite-system DMRG [16] can resolve this problem.

Increasing D/J further, a quantum phase transition occurs between EH and AFM phases. A discontinuous staggered magnetization suggests that this transition is of first order [7]. Quite recently, this was corroborated by analyzing the energy level crossing [33]. The numerically determined central charge $c^*(L)$ at $D/J = 3.7$ yields a further signature of the first-order transition [see Fig. 9(b)]. For small system sizes ($L = 32$), c^* shows a peak at $J_z/J \simeq 3.945$, in accord with the EH-AFM transition point in Ref. [33]. With increasing the system size L, c^* decreases drastically and becomes already zero for $L = 128$, which confirms the results of former studies [7,33].

C. Ground-state phase diagram

Figure 10 displays the DMRG ground-state phase diagram of the spin-1 XXZ model with single-ion anisotropy. The EH-OH and OH-AFM phase boundaries can been derived from central charge c^*, as explained above: Again we obtain a very good agreement with former ED and DMRG data [7,34]. Most notably, the nontrivial OH phase appears in between the trivial EH and AFM phases, just as the topological HI phase develops between the MI and DW phases in the EBHM. Therefore, we have included in Fig. 10 the phase boundaries of the MI-HI and HI-DW transitions for the EBHM with $n_b = 2$ (taken from Ref. [18]). Qualitatively, the phase diagram of the spin-1 model looks quite similar to those of the EBHM, except for the existence of the superfluid (SF) phase in the EBHM (not shown). Quantitatively, the topological phase of the EBHM captures a larger region in parameter space than the OH phase, however. This might be caused by the particle-hole symmetry-breaking term $\hat{\mathcal{H}}'$ in Eq. (4).

D. Dynamical structure factor

Let us finally discuss the spin dynamical properties of the spin-1 XXZ model.

Figure 11 reveals our DDMRG results for $S^{zz}(k,\omega)$ obtained for the spin-1 model (with anisotropy $D/J = 1.5$) inside the three insulating phases, as well as at the quantum phase transition points in between. In the EH phase, at $J_z/J = 1$, most of the spectral weight is concentrated in the momentum range $\pi/2 < k < \pi$ [see Fig. 11(a)]. The excitation gap appears at $k \approx 0$. The dispersion of the maximum in $S^{zz}(k,\omega)$ behaves cosinelike for small-to-intermediate momenta, and is flattened close to the Brillouin zone boundary (above $k \gtrsim 3\pi/4$). With increasing J_z/J, the EH-OH transition occurs at $J_z/J = J_{z,c1}/J \simeq 1.694$, where the excitation gap closes at the momentum $k = 0$, as shown in Fig. 11(b). Deep in the Haldane phase, the situation changes drastically [see Fig. 11(c) for $J_z/J = 1.9$]. Now the dispersion of the maximum in $S^{zz}(k,\omega)$ takes a sinelike form. Again there are finite excitation gaps at $k = 0$ (Haldane gap) and π. This resembles the behavior found at the isotropic Heisenberg point [30]. Here the spectral weight exclusively concentrates at $k \approx \pi$ and finite but small $\omega \ll J$. We finally ask whether the gap in $S^{zz}(k,\omega)$ again

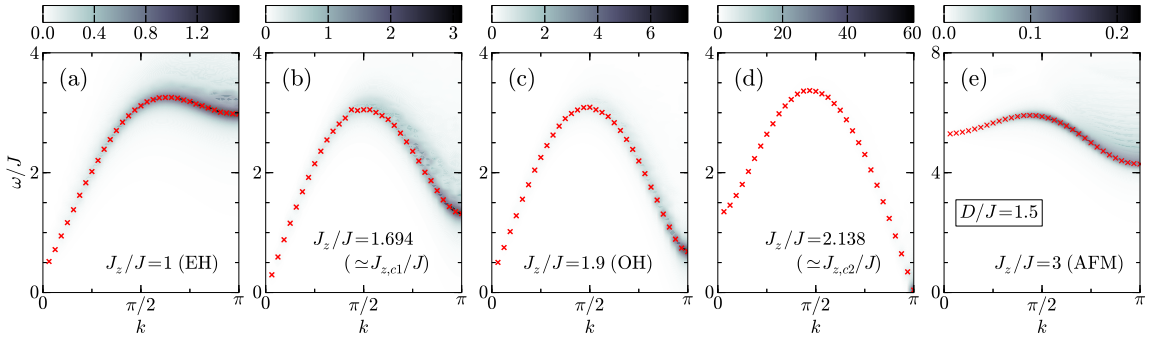

FIG. 11. (Color online) Intensity plots of the dynamical structure factor $S^{zz}(k,\omega)$ for (a) $J_z/J = 1$, (b) $J_z/J = 1.694 \simeq J_{z,c1}/J$, (c) $J_z/J = 1.9$, (d) $J_z/J = 2.138 \simeq J_{z,c2}/J$, and (e) $J_z/J = 3$. Data are obtained by the DDMRG technique for $L = 64$, using PBC and a Lorenzian broadening $\eta = 0.1t$. Crosses give the maximum value of $S^{zz}(k,\omega)$ at fixed momenta $k = 2\pi j/L$ with $j = 1,\ldots,L/2$.

closes at the OH-AFM transition if J_z/J is increased further. Figure 11(d) shows that the gap indeed closes, at $J_z/J = 2.138$ ($\simeq J_{z,c2}/J$), but this time at momentum $k = \pi$, reflecting the lattice-period doubling in the AFM phase. Obviously, $S^{zz}(k,\omega)$ follows the behavior of the neutral gap Δ_n shown in Fig. 5. In the AFM phase [see Fig. 11(e) with $J_z/J = 3$], the dispersion becomes flattened with a large excitation gap that opens at $k = \pi$, however. That is, the dynamical spin structure factor shows a distinct behavior in each phase of the spin-1 model with single-ion anisotropy. Interestingly, the results obtained in the EH, OH, and AFM phases are similar to those for the MI, HI, and DW phases of the 1D EBHM [18]. This corroborates that the spin-1 model can be taken as an effective model for the EBHM with $n_b = 2$.

V. SUMMARY

We studied the topological properties of the anisotropic spin-1 XXZ model with single-ion anisotropy in close analogy to a recent investigation of the extended Bose-Hubbard model (EBHM) with a nearest-neighbor repulsion [18]. The focus was on the nontrivial Haldane phase as well. The phase boundaries between trivial phases [even Haldane (EH) and AFM phases] and nontrivial odd Haldane (OH) phase were determined numerically with high precision via the central charge. The ground-state phase diagram resembles those of the restricted EBHM with a maximum number of bosons per site $n_b = 2$, but the topological phase takes a much narrower region in the parameter space. Simulating the spin and neutral gaps, which correspond to the single-particle respectively neutral gaps in the EBHM, we confirmed the closing of the gap at the trivial-nontrivial quantum phase transition as for the EBHM.

The degeneracy of the lowest entanglement level in the OH phase could be observed by finite-system DMRG calculations with both periodic (P) and open (O) boundary conditions (BC). With PBC the lowest level in the entanglement spectrum is fourfold degenerate in the OH phase; notably, the system-size dependence of the results is much stronger than for OBC. Adopting half spins ($S = 1/2$) at the open edges, the twofold degeneracy corresponding to a single artificial edge in the entanglement calculations can be detected easily. This degeneracy will be lifted turning on a finite perturbation that breaks the inversion symmetry of the lattice, independently from the BC used.

We furthermore used the dynamical DMRG technique to examine the dynamical spin structure $S^{zz}(k,\omega)$ which mimics the dynamical density fluctuations in the EBHM. In the topological $S = 1$ OH phase a sinus-shaped dispersion was observed for finite anisotropy D just as for the isotropic Heisenberg model and the Haldane-insulator state of the EBHM. Moreover, $S^{zz}(k,\omega)$ shows a significant different momentum and energy dependence in three different gapful phases for both the spin-1 model and the EBHM. We finally note that the influence of the particle-hole symmetry-breaking term $\hat{\mathcal{H}}'$ in Eq. (4) on the properties of the constrained EBHM is almost negligible, not only for static but also for dynamical quantities.

ACKNOWLEDGMENTS

The authors would like to thank Y. Fuji, F. Göhmann, F. Lange, S. Nishimoto, and F. Pollmann for valuable discussions. This work was supported by Deutsche Forschungsgemeinschaft (Germany), SFB 652, B5.

APPENDIX: HALDANE GAP

After Haldane's conjecture about the finite excitation gaps for integer-spin chains [1], it was a challenging issue to estimate these so-called Haldane gaps numerically (note that even the spin-1 XXZ Heisenberg chain is not integrable). White presented the first accurate DMRG results for the Haldane gap [20], and subsequently a series of more elaborated DMRG [21,38,40], quantum Monte Carlo (QMC) [37], and ED [39] studies have been performed. However, only OBC have been used within the DMRG framework so far, mainly because of the smaller computational costs. In this Appendix, we demonstrate—at least for the spin-1 Heisenberg model—that the Haldane gap can also be determined using PBC, and the system-size dependence of the gap is much smaller than those with OBC adopting the half-spin edges [cf. Fig. 1(b)]. Hence any finite-size scaling is needless.

Figure 12 presents the finite-size extrapolation of the corresponding spin and neutral excitation gaps, as defined in Sec. III B, for both OBC and PBC. The spin and neutral gaps

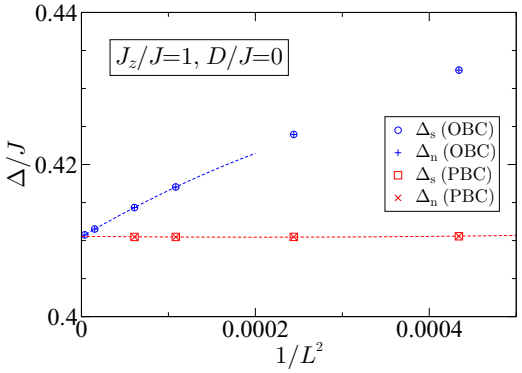

FIG. 12. (Color online) Finite-size scaling of the excitation gaps at the Heisenberg point ($D = 0$ and $J_z/J = 1$).

become equal (Δ) only at the Heisenberg point for $D = 0$ [cf. Fig. 5(a)]. Computing Δ for systems with up to $L = 512$ sites and OBC, we can extrapolate the results to the thermodynamic limit and obtain $\Delta = 0.410\,50(3)$ (in agreement with Ref. [38]). On the other hand, the first excitation gaps $\Delta = 0.410\,479\,24(4)$ obtained with PBC and up to $m = 4800$ density-matrix states show almost no finite-size dependence; see also the raw data for $L = 96$ and $L = 128$ in Table I. This value is very close to the (low-temperature) QMC [37] and ED [39] results and shows a perfect agreement with the very recent non-Abelian DMRG data with OBC [40]. Let us emphasize that although the accessible system size is rather limited for PBC, Δ for PBC is always lower than for OBC. Most notably, the system-size dependence is almost negligible (for enough large L), so that sophisticated extrapolation techniques or the use of special boundary conditions [39,40] are no longer mandatory for analyzing the Haldane gap in spin-1 chains.

TABLE I. First excitation gap Δ in the spin-1 XXZ chain as obtained by QMC, ED, and DMRG for a system size L, at temperature T, using the specified boundary conditions BC.

Method	L	Δ	T	BC
QMC [37]	128	0.41048(6)	0.015625	PBC
DMRG [38]	120	0.41050(2)	0	OBC
ED [39]	24	0.41047(8)	0	TBC
DMRG [40]	2048	0.4104792485(4)	0	OBC
DMRG (this work)	96	0.4104792(7)	0	PBC
DMRG (this work)	128	0.41047924(4)	0	PBC

[1] F. D. M. Haldane, Phys. Rev. Lett. **50**, 1153 (1983).
[2] W. J. L. Buyers, R. M. Morra, R. L. Armstrong, M. J. Hogan, P. Gerlach, and K. Hirakawa, Phys. Rev. Lett. **56**, 371 (1986).
[3] J. P. Renard, M. Verdaguer, L. P. Regnault, W. A. C. Erkelens, J. Rossat-Mignod, and W. G. Stirling, Europhys. Lett. **3**, 945 (1987).
[4] S. Ma, C. Broholm, D. H. Reich, B. J. Sternlieb, and R. W. Erwin, Phys. Rev. Lett. **69**, 3571 (1992).
[5] I. Affleck, T. Kennedy, E. H. Lieb, and H. Tasaki, Phys. Rev. Lett. **59**, 799 (1987).
[6] T. Kennedy and H. Tasaki, Phys. Rev. B **45**, 304 (1992).
[7] W. Chen, K. Hida, and B. C. Sanctuary, Phys. Rev. B **67**, 104401 (2003).
[8] K. Nomura, J. Phys. A **28**, 5451 (1995).
[9] Z.-C. Gu and X.-G. Wen, Phys. Rev. B **80**, 155131 (2009).
[10] F. Pollmann, A. M. Turner, E. Berg, and M. Oshikawa, Phys. Rev. B **81**, 064439 (2010).
[11] T. Tonegawa, K. Okamoto, H. Nakano, T. Sakai, K. Nomura, and M. Kaburagi, J. Phys. Soc. Jpn. **80**, 043001 (2011).
[12] K. Okamoto, T. Tonegawa, H. Nakano, T. Sakai, K. Nomura, and M. Kaburagi, J. Phys.: Conf. Ser. **302**, 012014 (2011).
[13] K. Okamoto, T. Tonegawa, H. Nakano, T. Sakai, K. Nomura, and M. Kaburagi, J. Phys.: Conf. Ser. **320**, 012018 (2011).
[14] Y.-C. Tzeng, Phys. Rev. B **86**, 024403 (2012).
[15] F. Pollmann, E. Berg, A. M. Turner, and M. Oshikawa, Phys. Rev. B **85**, 075125 (2012).
[16] J. A. Kjäll, M. P. Zaletel, R. S. K. Mong, J. H. Bardarson, and F. Pollmann, Phys. Rev. B **87**, 235106 (2013).
[17] E. G. Dalla Torre, E. Berg, and E. Altman, Phys. Rev. Lett. **97**, 260401 (2006).
[18] S. Ejima, F. Lange, and H. Fehske, Phys. Rev. Lett. **113**, 020401 (2014).
[19] E. Berg, E. G. Dalla Torre, T. Giamarchi, and E. Altman, Phys. Rev. B **77**, 245119 (2008).
[20] S. R. White, Phys. Rev. Lett. **69**, 2863 (1992).
[21] S. R. White, Phys. Rev. B **48**, 10345 (1993).
[22] E. Jeckelmann and H. Fehske, Riv. Nuovo Cimento **30**, 259 (2007).
[23] E. G. D. Torre, J. Phys. B: At. Mol. Opt. Phys. **46**, 085303 (2013).
[24] E. Jeckelmann, Phys. Rev. B **66**, 045114 (2002).
[25] H. J. Schulz, Phys. Rev. B **34**, 6372 (1986).
[26] M. den Nijs and K. Rommelse, Phys. Rev. B **40**, 4709 (1989).
[27] H. Li and F. D. M. Haldane, Phys. Rev. Lett. **101**, 010504 (2008).
[28] P. Calabrese and J. Cardy, J. Stat. Mech. (2004) P06002.
[29] S. Nishimoto, Phys. Rev. B **84**, 195108 (2011).
[30] M. Takahashi, Phys. Rev. B **50**, 3045 (1994).
[31] S. R. White and I. Affleck, Phys. Rev. B **77**, 134437 (2008).
[32] A. Kitazawa, K. Nomura, and K. Okamoto, Phys. Rev. Lett. **76**, 4038 (1996).
[33] G.-H. Liu, W. Li, W.-L. You, G. Su, and G.-S. Tian, Physica B **443**, 63 (2014).
[34] H. Ueda, H. Nakano, and K. Kusakabe, Phys. Rev. B **78**, 224402 (2008).
[35] A. Kitazawa and K. Nomura, J. Phys. Soc. Jpn. **66**, 3379 (1997).
[36] A. Kitazawa and K. Nomura, J. Phys. Soc. Jpn. **66**, 3944 (1997).
[37] S. Todo and K. Kato, Phys. Rev. Lett. **87**, 047203 (2001).
[38] S. R. White and D. A. Huse, Phys. Rev. B **48**, 3844 (1993).
[39] H. Nakano and A. Terai, J. Phys. Soc. Jpn. **78**, 014003 (2009).
[40] H. Ueda and K. Kusakabe, Phys. Rev. B **84**, 054446 (2011).